Insights into superconductivity of LaO from experiments and first-principles calculations

H. Gan,[1] C. Zhang,[2] X. Z. Du,[1] P. Jiang,[1,4] C. P. Niu,[1,3] X. H. Zheng,[1,3] Y. W. Yin,[1,*] and X. G. Li[1,5,†]

[1]*Hefei National Laboratory for Physical Sciences at the Microscale, Department of Physics, and CAS Key Laboratory of Strongly-Coupled Quantum Matter Physics, University of Science and Technology of China, Hefei 230026, China*

[2]*Instrumentation and Service Center for Physical Sciences, Westlake University, Hangzhou 310024, China*

[3]*Key Laboratory of Materials Physics, Institute of Solid State Physics, HFIPS, Chinese Academy of Sciences, Hefei 230031, China*

[4]*School of Physics and Electronic Engineering, Jiangsu Normal University, Xuzhou 221116, China*

[5]*Collaborative Innovation Center of Advanced Microstructures, Nanjing 210093, China*

(Received 8 April 2021; revised 30 July 2021; accepted 6 August 2021; published 23 August 2021)

To explore the mechanism of superconductivity in lanthanum monoxide (LaO) film, using first-principles calculations we investigated the electronic properties, phonon vibration, and electron-phonon coupling characteristics in LaO with a tetragonally distorted rocksalt structure in accordance with our experiments. It is demonstrated that LaO shows coexisting metallic and ionic characteristics, and the electronic density of states at the Fermi level is primarily from La-*d* and O-*p* orbitals. The low-frequency phonons from La atoms dominate 61% of the electron-phonon coupling constant, and the high-frequency phonons derived from O atoms contribute the rest. The calculated T_c of about 5.37 K is consistent with the experimental result, indicating that the superconductivity in LaO can be clearly illustrated by the phonon-mediated mechanism and McMillan's formula. The calculated results reveal that comparing LaO with other lanthanum monochalcogenides, the electronic properties vary more significantly than the phonon properties and lead to a stronger electron-phonon coupling in LaO, which is responsible for its higher T_c. The theoretical and experimental investigations provide deep insights into the mechanism of superconductivity in the LaO system.

DOI: 10.1103/PhysRevB.104.054515

I. INTRODUCTION

Lanthanum is an important element in superconducting materials, from the superconducting La [1], lanthanum compounds such as LaX (X = S, Se, or Te) [2], LaH_{10} [3], LaBi [4], LaSb [5], La_2Ni_2In [6], etc., to complex La-doped copper-based oxides [7–10]. Due to the similar structure of different lanthanum monochalcogenides LaX, experimental and theoretical investigations on their physical properties with X varying from S, Se, to Te have attracted much attention [11–13], which may provide valuable hints on how to uncover the mechanism of superconductivity. For example, from LaS, LaSe, to LaTe, it was found that the binding energy for the bottom of the conduction band decreases while the binding energy for the top of the valence band increases, confirmed by angle-resolved photoemission spectroscopy measurements [14]. The local spin-density approximation calculations indicate that the p bandwidth increases monotonically due to the enhancing extension of the atomic np wave function with increasing lattice constant [15]. The density of states (DOS) at the Fermi level, $N(E_F)$, calculated by the linear muffin-tin orbital method, increases with the increase of the atomic radius from S to Te [2]. Meanwhile, their Fermi surfaces are all in a nearly ellipsoidal shape centering at the X points in the Brillouin zone (BZ) [16]. Furthermore, the electronic band structure shows a similar line shape; the bond between La and X atoms is predicted to be both metallic as well as ionic [2]; and a clear band gap exists between optical and acoustic phonons for LaX (by the generalized gradient approximation) [17,18].

In addition to the properties mentioned above, the LaX compounds exhibit superconductivity with superconducting transition temperatures $T_c \sim$ 1–2 K. To understand the mechanism of superconductivity in LaX, theoretical calculations [2,11,13] have been carried out based on density functional theory. Considering McMillan's formula within the framework of Bardeen-Cooper-Schrieffer (BCS) theory [19], the calculations have revealed that LaX are conventional superconductors and their superconductivity can be described by the phonon-mediated electron-phonon interaction [2]. As a result of the theoretical calculations in LaX, the electron-phonon coupling (EPC) constant λ decreases from LaS, LaSe, to LaTe [2]. Typically, T_c is closely associated with the strength of EPC, and generally the T_c value increases with increasing λ but decreases with increasing molecular mass in LaX [2].

It is notable that the element O belongs to the same main group as S, Se, and Te, and it has a smaller atomic mass and atomic radius compared with other chalcogen atoms. Hence, LaO should be superconducting as well and may exhibit stronger superconductivity than LaX, which was experimentally demonstrated very recently in the LaO thin films with $T_c \sim$ 5 K [20]. The superconductivity of LaO thin films can be tuned by the stress from substrates, and the T_c of LaO

*Author to whom all correspondence should be addressed: yyw@ustc.edu.cn

†lixg@ustc.edu.cn

film decreases with the decrease of the unit-cell volume [20]. It can be seen that the T_c of LaO is approximately twice as high as that of LaX, and thus the theoretical investigations of electronic and phonon properties of LaO would be important for understanding its enhanced superconductivity. However, the mechanism behind the higher T_c in LaO is unclear, and corresponding theoretical calculations have not been carried out yet.

In this paper, we successfully grew superconducting LaO epitaxial films on $LaAlO_3$ substrates with $T_c \sim 5.27$ K. Theoretical investigations of the electron localization function (ELF) and the differential charge density (DCD) indicate the coexistence of metallic and ionic characters in LaO. In particular, LaO was found to be a conventional superconductor, and its T_c was calculated to be 5.37 K, consistent with the experimental observation. The calculations reveal that the higher T_c in LaO than LaX is related to its stronger electron-phonon coupling, which is mainly attributed to the peculiar electronic properties.

II. METHODS

A. Experiment

Epitaxial LaO (001) films on commercial $LaAlO_3$ (001) substrates were grown by ablating a bulk La metal target (purity ~99.99%) using a pulsed laser deposition technique with a KrF laser (248 nm wavelength). Before deposition, the chamber was purged three times with high-purity nitrogen gas, and the base pressure of the chamber was about 2×10^{-5} Pa. The deposition temperature, target-substrate distance, and laser energy density were 300 °C, 4.0 cm, and 2.5 J cm^{-2}, respectively. After deposition, the substrate was cooled down naturally in the high vacuum. Then, a ~50-nm-thick AlO_x capping layer was deposited *in situ* onto the film surface at room temperature to prevent the oxidation of LaO in air, and the typical thickness of LaO film was approximately 150 nm, as revealed by cross-sectional scanning electron microscopy (SEM). The crystal structure for LaO film was identified by means of x-ray diffraction (XRD) with Cu Kα1 radiation at a wavelength of 1.5406 Å. The resistances were measured by using a standard four-probe technique in the Physical Property Measurement System (PPMS-9T, Quantum Design).

B. Calculation

The electronic structure was calculated by utilizing the density functional theory, which is on the basis of a generalized gradient approximation (GGA) with a Perdew-Burke-Ernzerhof (PBE) functional [21]. The calculations have been performed using the code QUANTUM ESPRESSO [22,23]. The kinetic energy cutoff for the wave functions expanded on a plane-wave basis set was 60 Ry, and the kinetic energy cutoff for potential and charge density was 720 Ry. The ultrasoft Vanderbilt pseudopotential was used to model the core-valence interaction. The Methfessel-Paxton smearing [24] with a width of 0.02 Ry was taken into consideration by integrating in the first BZ to determine the electronic properties. We used the Broyden-Fletcher-Goldfarb-Shanno (BFGS) algorithm [25,26] to fully relax the crystal structure and the atomic coordinates in order to ensure that the maximum force was below 10^{-6} Ry/Bohr on each atom. A $12 \times 12 \times 12$ Monkhorst-Pack mesh was used to calculate the electronic band structure, while a finer $60 \times 60 \times 60$ mesh was used to calculate the DOS connecting the special high symmetry k-points in the first BZ. The dynamic matrix and electron-phonon coupling were computed using a grid of $5 \times 5 \times 5$ mesh for phonon wave vectors and a grid of $40 \times 40 \times 40$ mesh for finer k point convergence, respectively. The phonon dispersion curves, phonon DOS, and electron-phonon interactions were calculated within the frame of density functional perturbation theory (DFPT) [27]. The electronic band structures and phonon dispersions of LaO were also studied using the GGA-PBE functional and the Heyd-Scuseria-Ernzerhof (HSE06) [28] hybrid functional by the Vienna *ab initio* simulation package (VASP) [29,30] to reveal the impact of using different exchange-correlation functionals. The related results are shown in the Supplemental Material [31].

The Allen-Dynes modified McMillian equation [19,32,33] was used to estimate the superconducting transition temperature (T_c):

$$T_c = \frac{\omega_{\ln}}{1.20} \exp\left(-\frac{1.04(1+\lambda)}{\lambda - \mu^*(1+0.62\lambda)}\right), \tag{1}$$

where μ^* is the Coulomb coupling constant, $\omega_{\ln}$ is the logarithmically averaged phonon frequency, and λ is the EPC constant. The last two parameters can be calculated as follows [32,33]:

$$\omega_{\ln} = \exp\left(\frac{2}{\lambda}\int_0^\infty \alpha^2F(\omega)\ln\omega\frac{d\omega}{\omega}\right), \tag{2}$$

$$\lambda = 2\int_0^\infty \frac{\alpha^2F(\omega)}{\omega}d\omega, \tag{3}$$

where $\alpha^2F(\omega)$ is the Eliashberg spectral function [33]:

$$\alpha^2F(\omega) = \frac{1}{2\pi N(E_F)}\sum_{\mathbf{q}\nu}\delta(\omega-\omega_{\mathbf{q}\nu})\frac{\gamma_{\mathbf{q}\nu}}{\hbar\omega_{\mathbf{q}\nu}}, \tag{4}$$

in which $N(E_F)$, $\gamma_{\mathbf{q}\nu}$, and $\omega_{\mathbf{q}\nu}$ are the DOS at Fermi level E_F, the phonon linewidth, and the frequency of ν phonon mode at the wave vector $\mathbf{q}$, respectively. $\gamma_{\mathbf{q}\nu}$ is defined by [33]

$$\gamma_{\mathbf{q}\nu} = 2\pi\omega_{\mathbf{q}\nu}\sum_{\mathbf{k}nn'}\left|g^{\mathbf{q}\nu}_{\mathbf{k}+\mathbf{q}n',\mathbf{k}n}\right|^2\delta(E_{\mathbf{k}n}-E_F)\delta(E_{\mathbf{k}+\mathbf{q}n'}-E_F), \tag{5}$$

where $g^{\mathbf{q}\nu}_{\mathbf{k}+\mathbf{q}n',\mathbf{k}n}$ is the EPC matrix element.

III. RESULTS AND DISCUSSION

A. Superconducting properties of LaO in experiments

Figure 1(a) shows the XRD $\theta-2\theta$ specular scan of an as-grown LaO film on $LaAlO_3$ (001) substrate. The (002) and (004) diffraction peaks of LaO film and the (00l) diffraction peaks of $LaAlO_3$ substrate were clearly observed, demonstrating the (001) out-of-plane orientation of LaO film. The rocking curve of the LaO (002) peak depicted in Fig. 1(b) demonstrates that the full width at half-maximum (FWHM) is ~0.47°, indicating a fairly good crystallinity of LaO film. The XRD $\theta-2\theta$ scan pattern around the LaO (111) peak was also measured at an inclination angle ψ of ~54.73°, as shown in Fig. 1(c). Based on the 2θ values of the (004) and (111)

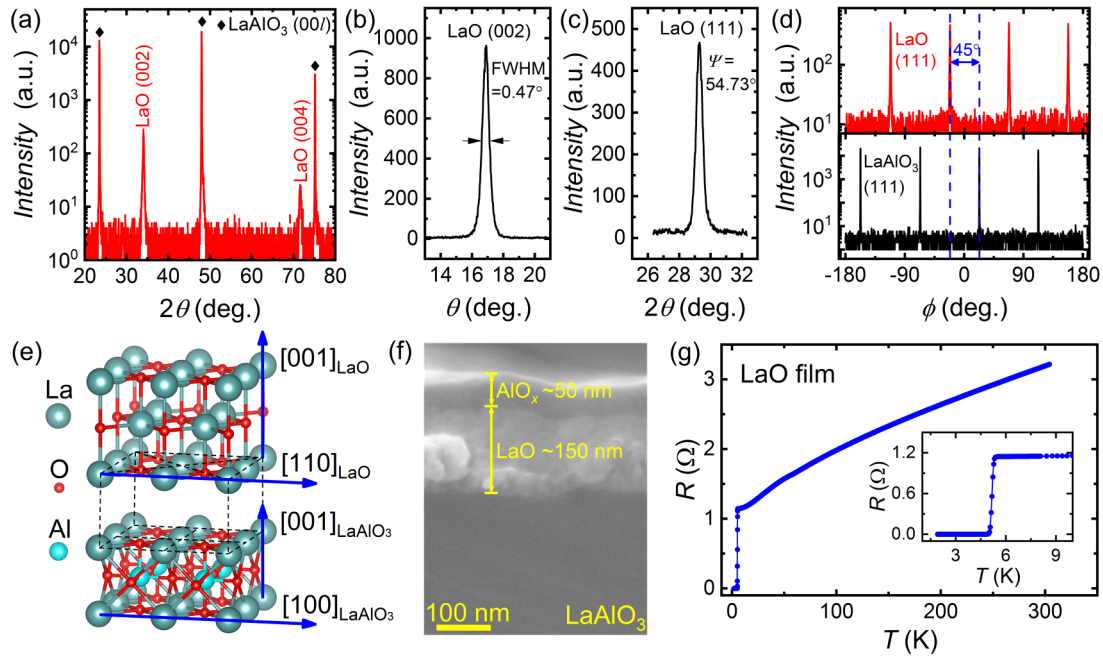

FIG. 1. (a) XRD $\theta-2\theta$ pattern for LaO film on $LaAlO_3$ (001) substrate. (b) Rocking curve for LaO (002) reflection. (c) XRD $\theta-2\theta$ scan pattern around LaO (111) peak. (d) XRD ϕ-scans of LaO (111) and $LaAlO_3$ (111) planes. (e) Schematic crystal structure of the LaO film on the $LaAlO_3$ substrate. (f) Cross-sectional SEM image of the specimen. (g) Temperature-dependent resistance of LaO film. The inset shows the enlarged view near the superconducting transition.

peaks, the lattice constants of the LaO film can be calculated as $a = b = 5.295$ Å and $c = 5.266$ Å. Therefore, a tetragonal distortion occurs when the lanthanum monoxide film is grown on the $LaAlO_3$ substrate, similar to the earlier report [20]. The distortion might result from the in-plane tensile strain from the substrate. The XRD ϕ-scans of LaO (111) and $LaAlO_3$ (111) planes in Fig. 1(d) show four distinct peaks at 90° intervals to each other with nearly the same intensity, revealing a fourfold rotational symmetry along the LaO (001) plane normal and the $LaAlO_3$ (001) plane normal. According to the ϕ difference ~45° between the LaO (111) and $LaAlO_3$ (111) peaks, the in-plane epitaxial relationship can be determined as LaO [110]//$LaAlO_3$ [100], as schematically shown in Fig. 1(e). The cross-sectional SEM image of LaO indicates that the thicknesses of LaO and AlO_x are ~150 and ~50 nm, respectively, as shown in Fig. 1(f).

The superconductivity in LaO film was unambiguously confirmed by its zero resistance, as the temperature-dependent resistance from 2 to 300 K shown in Fig. 1(g). In the normal state, the resistance decreases with decreasing temperature, indicating the metallic nature of LaO. When the temperature goes down further, the resistance shows a sharp decrease, and a superconducting behavior appears with the onset superconducting transition temperature $T_{c,onset} \sim 5.27$ K (defined by the criterion of 90% of the normal-state resistance [34]) and the zero-resistance temperature $T_{c,zero} \sim 4.87$ K, similar to the earlier report on LaO film of $T_c \sim 5$ K [20].

B. Superconducting properties of LaO via first-principles calculations

It can be seen that the T_c of LaO is higher than other lanthanum monochalcogenides. To reveal the physical mechanism of the enhanced superconductivity, it is necessary to calculate the electronic, phonon, and electron-phonon coupling properties of LaO for further elucidating its superconductivity using density functional theory. According to the experimental results, the LaO shows a distorted rocksalt structure when it grows as a thin film on the substrate, which causes the LaO to be a tetragonal structure in the $I4/mmm$ (no. 139) space group. The lattice constants of tetragonal LaO relaxed by first-principles calculations are $a = b = 5.1335$ Å and $c = 5.1331$ Å.

LaO with a tetragonal structure contains one lanthanum atom positioned at (0,0,0) and one oxygen atom positioned at (0,0.5,0.5) in fractional coordinates per primitive cell. To explore the bonding character of LaO, the ELF [35] and the DCD (charge density minus superposition of atomic densities) of the system were calculated. ELF is an effective way for bond classification, and it can be described in a map of real space in the range between 0 and 1, where 0 corresponds to a completely nonlocal state, 0.5 to a uniform electron gas, and 1 to a perfect localization state. Figures 2(a)–2(f) present the ELF and DCD calculated in three particular slices of LaO, i.e., for the slices containing only La atoms [Figs. 2(a) and 2(d)], only O atoms [Figs. 2(b) and 2(e)], and both La and O atoms [Figs. 2(c) and 2(f)], respectively. It is found clearly in Fig. 2(a) that the maximum ELF value in the central triangle among the La atoms approaches 0.59, demonstrating a strong metallic bonding. The ELF values of triangular regions are around 0.4-0.6 among O atoms as shown in Fig. 2(b), which also indicates the metallic character. However, as depicted in Fig. 2(c), the maximum ELF value of the narrow channel between La and O is less than 0.2, and there is an apparent difference between the lower ELF value of the La region and the higher ELF value of the O region. This indicates the

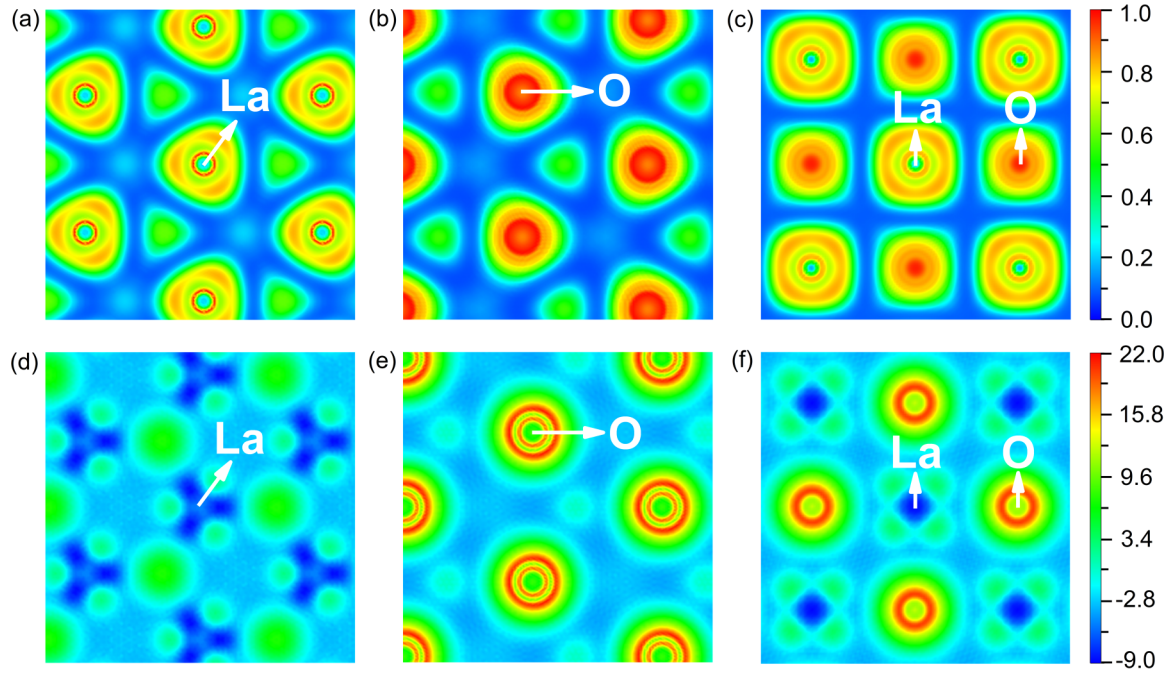

FIG. 2. (a)–(c) Electron localization function maps in the (111) plane (a), (b) and the (001) plane (c) of LaO, respectively. (d)–(f) Differential charge density (10^{-3} e/Bohr^3) maps in the (111) plane (d), (e) and the (001) plane (f) of LaO, respectively.

existence of recognized ionic bonds rather than covalent bonds in the LaO. It should be noted that the higher ELF values of the residual channels in the interstitial region between La and O atoms demonstrate that the metallicity still exists with the ionicity in this slice.

The DCD map in Fig. 2(d) shows that the charge density around La atoms is very low, but the charge density of the spherical region is relatively high, indicating that La atoms lose charges. Figure 2(e) depicts that the charge density around O atoms is very high, indicating that O atoms gain charges. This means that La and O atoms act as charge donors and acceptors, respectively, and the charges transfer from La atoms to O atoms, as shown in Fig. 2(f). Overall, the ELF and DCD results reveal that the metallic bonds are formed in LaO, consistent with our experimental results, and there is also a non-negligible ionicity between La and O atoms.

The metallic nature of LaO is also confirmed by the calculated electronic band structure in Fig. 3(a) which shows that the conduction-band bottom is about 2.51 eV below the Fermi level. There are three valence bands between −6.48 and −3.82 eV. These valence bands give rise to two peaks at −5.76 and −4.45 eV in the electronic DOS. As shown in Fig. 3(b), the lower parts of three valence bands are predominantly due to the La-d and O-p orbitals. In the wide range of conduction bands, La-d electrons dominate the DOS and strongly hybridize with O-p electrons while La-s, La-p, and O-s electrons contribute to the rest. In addition, the two peaks at −0.55 and 0.66 eV are mainly contributed by La atoms in the electronic DOS, which clearly indicates that La electrons dominate in the conduction band. The calculated $N(E_F) \sim 0.55$ states/eV/f.u. of LaO is lower than other lanthanum monochalcogenides, and these $N(E_F)$ follow the trend that the $N(E_F)$ decreases with the decrease of the atomic number of chalcogen [2,11]. This may be due to the enhanced overlapping between the La-d and O-p or X-p orbitals with the reduced interatomic separation from LaTe to LaO. The broadening of the d-bands is a consequence of this enhancement of the d-p hybridization, which results in a lower DOS at the Fermi level [2]. We noted that the hybridization between the La and O atoms is stronger than that between La and S (or Se/Te) in LaX [2,11], which is closely related to the following aspects: (i) The electronegativity of O (3.44 eV) is larger than S (2.58 eV), Se (2.55 eV), and Te (2.10 eV), and the bonding strength at 298 K of La-O (798 kJ/mol) is stronger than those of La-S (573.4 ± 1.7 kJ/mol), La-Se (485.7 ± 14.6 kJ/mol), and La-Te (385.6 ± 15 kJ/mol) [36]. Thus, the combination of La and O will be relatively stronger [36]. (ii) The calculated conduction-band width of LaO is ∼2.52 eV in our work, which is larger than those of LaS (2.38 eV), LaSe (2.15 eV), and LaTe (1.85 eV) [2]. This demonstrates the greater hybridization in the case of LaO than LaX [2,37]. (iii) The lattice constant of LaO is the smallest among these compounds, which is closely related to the smallest atomic radius and the strongest electronegativity of the O atom. Hence, the hybridization can be expected to increase from LaX to LaO [11].

Figure 3(c) shows the Brillouin zone of the LaO lattice and the path calculated in the band structure along the special high-symmetry k-points $\Gamma, X, Y, \Sigma, \Gamma, Z, \Sigma_1, N, P, Y_1, Z$, and P. The Fermi level intersects only one band in all directions between the high-symmetry points of the BZ, indicating that there is only one Fermi surface. As shown in Fig. 3(d), the Fermi surface consists of six closed and disconnected electronlike pockets [38] and 12 small electronlike sheets. The six pockets are centered at points Z or X separately, similar to LaX [16]. Meanwhile, all of the pockets and sheets are integrally symmetrical around the center Γ point. In addition, it is noted that the disconnected pockets in LaO are similar to LaS and LaSe but slightly different from LaTe in which the

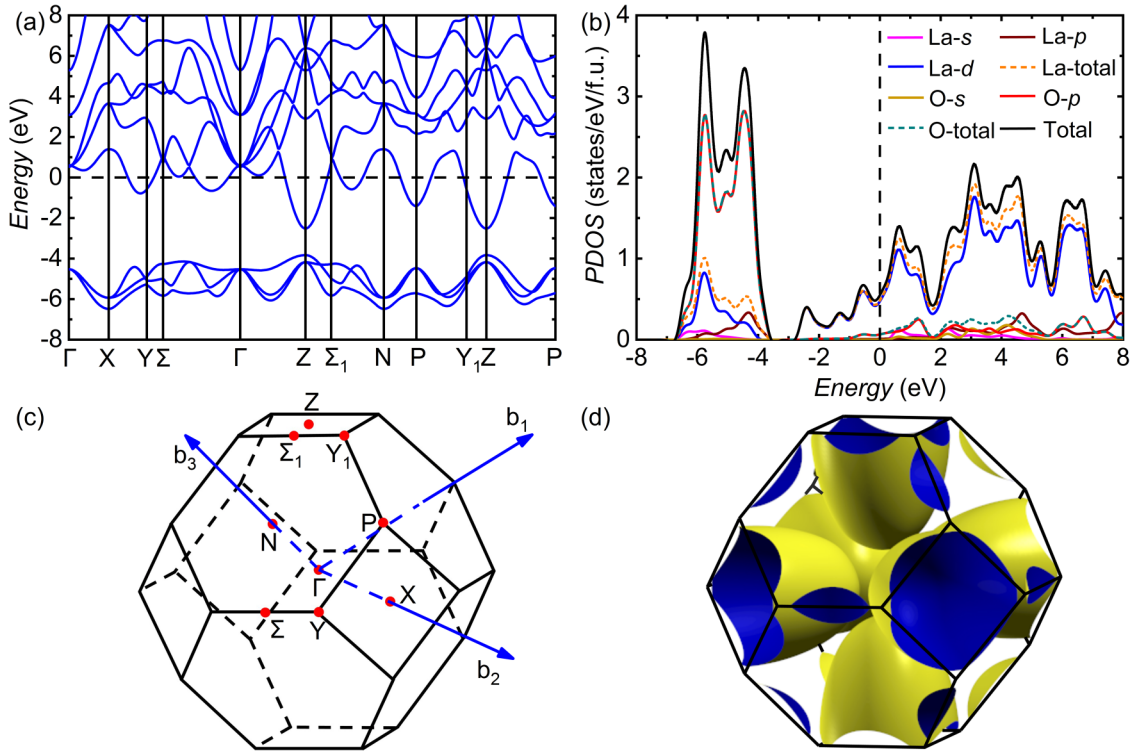

FIG. 3. (a) Electronic band structure of LaO plotted along Γ, X, Y, Σ, Γ, Z, Σ_1, N, P, Y_1, Z, and P high-symmetry k points. (b) Partial electronic density of states of LaO. The parallel (a) and perpendicular (b) dashed lines indicate the position of the Fermi level. (c) Brillouin zone of the LaO lattice. (d) Three-dimensional Fermi surface of the tetragonal LaO.

ellipsoidal electronlike pockets are connected at the Γ point [16].

The quantum-mechanical many-body state has been investigated for electron interaction in superconducting materials by using the BCS theory and introducing electron-phonon coupling. Studies have shown that Cooper pairs can be formed by electrons near the Fermi level and thus superconductivity may show up in materials [39]. Focusing on the vibrational properties, the phonon frequencies as well as the projected phonon DOS were calculated. Figure 4(a) shows six phonon branches including three acoustic branches and three optical branches. The dynamical stability of LaO is demonstrated by the phonon dispersion curves without imaginary frequency [39]. Along the special symmetry directions Y-Σ, Z-Σ_1, and Y_1-Z, the flatness of different branches increases in consideration of the symmetry. Notably, the acoustic and optic branches have a clear phonon dispersion band gap because an La atom is much heavier than an O atom (the mass ratio of M_{La}/M_O is equal to 8.68), as shown in Fig. 4(a). In this case, the vibrations of La atoms principally contribute to the acoustic phonon modes, while the vibrations of O atoms principally contribute to the optical phonon modes, as indicated by the projected phonon DOS shown in Fig. 4(b). On the one hand, the optical branches are relatively flat throughout the BZ except at X and N, resulting in the two peaks at the frequencies of 7.51 and 9.37 THz in the phonon DOS. On the other hand, along the

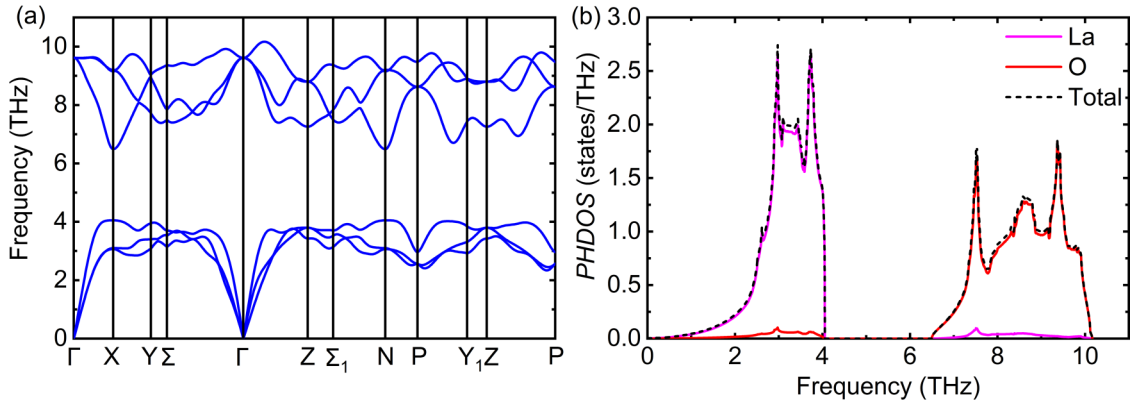

FIG. 4. (a) Phonon dispersion curves, and (b) projected phonon density of states of LaO.

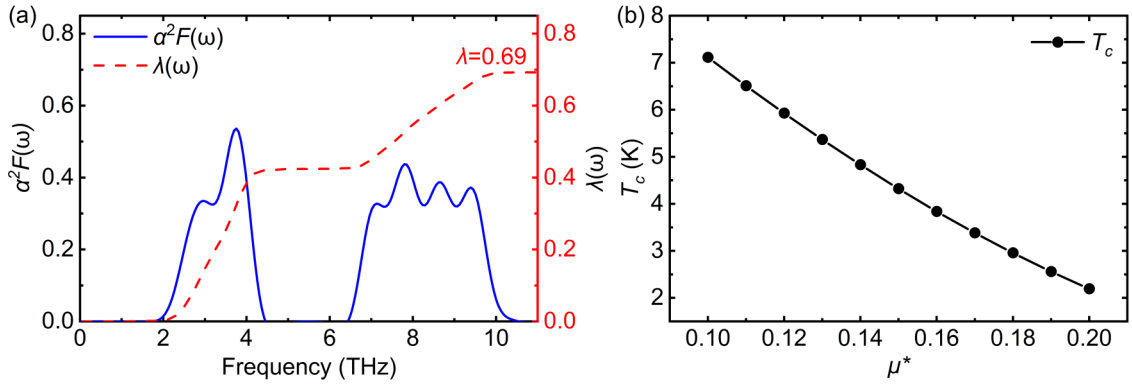

FIG. 5. (a) Eliashberg spectral function, $\alpha^2F(\omega)$ (solid line), and frequency-dependent electron-phonon coupling constant, $\lambda(\omega)$ (dashed line), of LaO. (b) Superconducting transition temperature T_c as a function of μ^*.

Y-Σ, Z-Σ_1, and Y_1-Z directions, the flatness of acoustic phonon branches leads to the two sharp peaks at frequencies of 2.97 and 3.74 THz in the phonon DOS. It is worth mentioning that there is no longitudinal optical and transverse optical (LO-TO) splitting in the phonon dispersion. Generally, the LO-TO splitting is caused by the long-range Coulomb interaction [40,41], which typically exists in insulators or semiconductors [41–44]. While in metallic systems, the long-range Coulomb interaction would be efficiently screened [45,46] and thus the LO-TO splitting will be absent. In our case, LaO is of metallic behavior and the long-range Coulomb interaction could be screened. Thus, the LO and TO branches are triply degenerated at the Γ point; see, e.g., the phonon dispersions shown in Fig. 4(a). This is consistent with the calculated results on LaX [17,18]. In addition, from our calculation results by VASP (see the Supplemental Material [31] for details), it can be seen that with the GGA and HSE functionals, the electronic band structures near the Fermi level are almost identical, and the low-frequency phonons are very similar. This suggests that the calculation on the superconducting properties would not be overtly affected with different functionals [47].

To investigate the superconductivity in LaO, the phonon frequency-dependent Eliashberg spectral function $\alpha^2F(\omega)$ and EPC constant λ are calculated by using Eqs. (4) and (3), respectively, as depicted in Fig. 5(a). Comparing Fig. 5(a) with Fig. 4(b), the similar curve shape between $\alpha^2F(\omega)$ and the phonon DOS indicates that all vibration frequencies contribute to the electron-phonon coupling. There are two main ranges of phonon energies contributing to the EPC constant λ: the lower phonon frequencies from 1.82 to 4.48 THz and the higher phonon frequencies from 6.41 to 10.50 THz. Specifically, the EPC constant λ is dominated by two aspects: (i) The lower-energy phonons coupling with electrons related to the La atoms contribute approximately 61% of the total λ value. (ii) The remaining 39% mainly comes from the higher-energy phonons coupling with electrons associated with O atoms. The electron-phonon coupling is due to the interactions of these phonons with the electrons from La-d and O-p states. Remarkably, the obtained total EPC constant λ of 0.69 is moderately large for superconductivity [48–50]. Based on the obtained $\alpha^2F(\omega)$ and λ, the logarithmic average of the phonon energy $\omega_{\ln} \sim 222.11$ K was obtained according to Eq. (2).

Figure 5(b) shows that the T_c calculated by Eq. (1) decreases with decreasing Coulomb coupling constant μ^* in the range from 0.1 to 0.2 [19]. Typically, the values of μ^* are usually 0.1–0.13 for various superconductors [32,51]. Here, the μ^* value of 0.13 is used for LaO, the same as that reported for LaX [2], and T_c of LaO is estimated to be about 5.37 K, very close to our experimental $T_c \sim 5.27$ K in Fig. 1(g). The factors such as structural defects or electron inhomogeneity in experiments and the overestimation of electronic DOS in calculations may cause the deviation between experimental observation and theoretical calculation [52]. It should be pointed out that the T_c of the LaO film (∼150 nm) measured by our experiment shown in Fig. 1(g) is in good agreement with our first-principles calculation as well as earlier experimental results on a ∼20 nm LaO film reported by Kaminaga *et al.* [20]. Generally, the physical properties including superconductivity of films tend to be close to the bulk ones when the film thickness is above a certain level (mostly tens of nanometers) [52–59]. Thus, it can be expected that the superconducting properties of our LaO film (150 nm) will be retained in the bulk one.

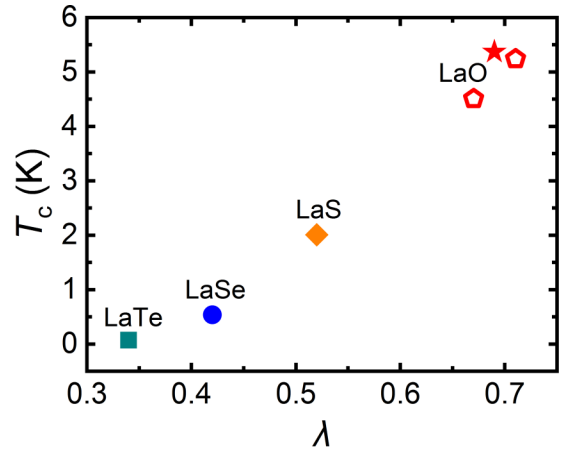

FIG. 6. Superconducting transition temperature T_c as a function of electron-phonon coupling constant λ for LaO and LaX. The solid points are from theoretical calculations of this work (red star) and an earlier report [2], and the hollow points are results derived from experimental data [20].

TABLE I. Theoretical calculated values of $N(E_F)$ (states/eV/f.u.), $\langle I^2\rangle$ [(eV/Å)^2], $M(1.661\times10^{-27}$ kg), $\langle\omega^2\rangle^{1/2}$ (K), η(eV/Å^2), κ(eV/Å^2), λ, and T_c (K).

Compound	$N(E_F)$	$\langle I^2\rangle$	M	$\langle\omega^2\rangle^{1/2}$	η	κ	λ	T_c	Ref.
LaO	0.55	26.33	154.91	276	14.48	20.99	0.69	5.37	This work
LaS	1.11	5.42	170.97	195	6.02	11.58	0.52	2.01	[2]
LaSe	1.24	3.50	217.88	163	4.34	10.33	0.42	0.54	[2]
LaTe	1.40	1.76	266.51	124	2.47	7.25	0.34	0.07	[2]

It should be pointed out that the theoretical results of both T_c and λ for LaO are in good agreement with the earlier reports derived experimentally by Kaminaga *et al.* [20], as depicted in Fig. 6. Interestingly, by comparing λ and T_c of LaO with the values from LaX [2], it is found that the values of λ increase monotonously from LaTe to LaO with decreasing the atomic number of chalcogen atoms, and the EPC constant contributes positively to obtaining a higher T_c in this system. It is known that the λ can be approximately expressed by [19]

$$\lambda = \eta/M\langle\omega^2\rangle. \tag{6}$$

Here, the Hopfield parameter $\eta = N(E_F)\langle I^2\rangle$ only describes the electronic characteristics, where $\langle I^2\rangle$ is the average square of the electronic matrix element over the Fermi level [19]; the force constant $\kappa = M\langle\omega^2\rangle$ corresponds to the phonon properties, where M is the mass and $\langle\omega^2\rangle$ is the average square of the phonon frequency. To obtain a comprehensive understanding of the variation trends of λ and T_c in Fig. 6, the values of $N(E_F)$, $\langle I^2\rangle$, M, $\langle\omega^2\rangle^{1/2}$, η, κ, λ, and T_c of LaO and LaX are listed in Table I. It can be seen from Table I that all these parameters change monotonously from LaTe to LaO. The $N(E_F)$ and M of LaO are the lowest, while its $\langle I^2\rangle$, $\langle\omega^2\rangle$, η, κ, λ, and T_c are the highest.

According to Eq. (6), both the increased electronic term η and the phonon term κ from LaTe to LaO compete with each other in affecting λ. On the one hand, although the $N(E_F)$ decreases from LaTe to LaO, the Hopfield parameter η undergoes a significant increase due to the higher $\langle I^2\rangle$, which contributes proportionally to the higher λ. On the other hand, from Te to O, the decrease of atomic radius and the increase of the electronegativity result in the decrease of interatomic spacing and the increase of bond strength from LaTe to LaO, and these lead to the phonon stiffening with higher $\langle\omega^2\rangle$, as obtained from the phonon property calculations [17,18]. Even though the M decreases from LaTe to LaO, the more profound increase in $\langle\omega^2\rangle$ results in the enhancement of the phonon term κ that is inversely proportional to λ. Overall, the much stronger increase in the electronic term η contributes more significantly to λ, explaining the larger λ as well as the higher T_c of LaO than those of other LaX.

The above calculation based on the BCS theory using the modified McMillian equation is in good agreement with the experimental results. As we know, the researchers have also concluded that LaX (X = S, Se, or Te) is a conventional BCS electron-phonon coupling superconducting system [2]. Even for the clathrate-like structured LaH_{10} with a superconducting transition temperature close to 250 K under high pressure, it is still considered as a conventional superconductor and its superconductivity can be described by BCS theory [3,60]. However, it is difficult to rule out non-BCS type mechanisms. For example, for some unconventional superconductors, such as lanthanum strontium copper oxide, some non-BCS mechanisms were proposed to explain the origin of the superconductivity, including the Anderson non-Fermi-liquid high-temperature superconducting mechanism [61], the Schrieffer spin bag mechanism [62,63], the nearly antiferromagnetic Fermi liquid mechanism [64,65], the bipolaron mechanism [66,67], etc. The non-BCS mechanisms have always been a challenging topic in condensed-matter physics, and further experimental and theoretical research is required.

IV. CONCLUSIONS

In summary, the superconductivity of LaO has been studied by experiments and first-principles calculations. The calculations on the electronic and phonon properties of LaO showed that La-d and O-p electrons dominate the electronic DOS at the Fermi level, and the tetragonally distorted rocksalt structure LaO is dynamically stable. Based on the calculation of electron-phonon coupling, La atoms mainly contribute to the low-frequency phonons which dominate the EPC constant λ. The stronger phonon-mediated EPC in LaO than LaX, mainly contributed from the significantly varied electronic contribution, makes its $T_c \sim 5.37$ K higher than other lanthanum monochalcogenides. The consistency of our experimental observations and theoretical calculations provides an understanding of the intrinsic superconducting properties of LaO.

ACKNOWLEDGMENTS

This work was supported by the National Key Research and Development Program of China (2019YFA0307900), the National Natural Science Foundation of China (51790491, 21521001, and 51972296), and the fundamental research funds for the central universities (WK2030000035). The numerical calculations in this paper have been performed on the supercomputing system in the Supercomputing Center of University of Science and Technology of China.

[1] W. H. Chen, D. V. Semenok, I. A. Troyan, A. G. Ivanova, X. L. Huang, A. R. Oganov, and T. Cui, Phys. Rev. B **102**, 134510 (2020).

[2] S. Sankaralingam, S. M. Jaya, G. Pari, and R. Asokamani, Phys. Stat. Sol. (b) **174**, 435 (1992).

[3] A. P. Drozdov, P. P. Kong, V. S. Minkov, S. P. Besedin, M. A. Kuzovnikov, S. Mozaffari, L. Balicas, F. F. Balakirev, D. E. Graf, V. B. Prakapenka, E. Greenberg, D. A. Knyazev, M. Tkacz, and M. I. Eremets, Nature (London) **569**, 528 (2019).

[4] J. F. Zhang, P. J. Guo, M. Gao, K. Liu, and Z. Y. Lu, Phys. Rev. B **101**, 155139 (2020).

[5] M. Zhang, X. Q. Wang, A. Rahman, R. C. Dai, Z. P. Wang, and Z. M. Zhang, Phys. Rev. B **101**, 064106 (2020).

[6] J. Maiwald, I. I. Mazin, A. Gurevich, and M. Aronson, Phys. Rev. B **102**, 165125 (2020).

[7] V. A. Gavrichkov, Y. Shan'ko, N. G. Zamkova, and A. Bianconi, J. Phys. Chem. Lett. **10**, 1840 (2019).

[8] J. J. Wen, H. Huang, S. J. Lee, H. Jang, J. Knight, Y. S. Lee, M. Fujita, K. M. Suzuki, S. Asano, S. A. Kivelson, C. C. Kao, and J. S. Lee, Nat. Commun. **10**, 3269 (2019).

[9] S. Kawasaki, Z. Li, M. Kitahashi, C. T. Lin, P. L. Kuhns, A. P. Reyes, and G. Q. Zheng, Nat. Commun. **8**, 1267 (2017).

[10] M. Dragomir, Q. L. Ma, J. P. Clancy, A. Ataei, P. A. Dube, S. Sharma, A. Huq, H. A. Dabkowska, L. Taillefer, and B. D. Gaulin, Phys. Rev. Mater. **4**, 114801 (2020).

[11] G. Vaitheeswaran, V. Kanchana, and M. Rajagopalan, J. Phys. Chem. Solids **64**, 15 (2003).

[12] G. Vaitheeswaran, V. Kanchana, S. Heathman, M. Idiri, T. Le Bihan, A. Svane, A. Delin, and B. Johansson, Phys. Rev. B **75**, 184108 (2007).

[13] J. Gao, Y. D. Liu, Q. L. Zhang, G. S. Qi, and W. Z. Jiao, J. Supercond. Novel Magn. **27**, 2455 (2014).

[14] M. Nakayama, T. Ito, H. Kumigashira, H. Matsui, H. Komatsu, T. Takahashi, H. Aoki, and A. Ochiai, J. Magn. Magn. Mater. **272–276**, E121 (2004).

[15] V. N. Antonov, B. N. Harmon, and A. N. Yaresko, Phys. Rev. B **69**, 094404 (2004).

[16] M. Nakayama, N. Kimura, H. Aoki, A. Ochiai, C. Terakura, T. Terashima, and S. Uji, Phys. Rev. B **70**, 054421 (2004).

[17] F. Soyalp, Comput. Mater. Sci. **43**, 313 (2008).

[18] F. Soyalp, Comput. Mater. Sci. **44**, 1371 (2009).

[19] W. L. McMillan, Phys. Rev. **167**, 331 (1968).

[20] K. Kaminaga, D. Oka, T. Hasegawa, and T. Fukumura, J. Am. Chem. Soc. **140**, 6754 (2018).

[21] J. P. Perdew, K. Burke, and M. Ernzerhof, Phys. Rev. Lett. **77**, 3865 (1996).

[22] P. Giannozzi, O. Andreussi, T. Brumme, O. Bunau, M. Buongiorno Nardelli, M. Calandra, R. Car, C. Cavazzoni, D. Ceresoli, M. Cococcioni, N. Colonna, I. Carnimeo, A. Dal Corso, S. de Gironcoli, P. Delugas, R. A. DiStasio, A. Ferretti, A. Floris, G. Fratesi, G. Fugallo, R. Gebauer, U. Gerstmann, F. Giustino, T. Gorni, J. Jia, M. Kawamura, H. Y. Ko, A. Kokalj, E. Kucukbenli, M. Lazzeri, M. Marsili, N. Marzari, F. Mauri, N. L. Nguyen, H. V. Nguyen, A. Otero-de-la-Roza, L. Paulatto, S. Ponce, D. Rocca, R. Sabatini, B. Santra, M. Schlipf, A. P. Seitsonen, A. Smogunov, I. Timrov, T. Thonhauser, P. Umari, N. Vast, X. Wu, and S. Baroni, J. Phys.: Condens. Matter **29**, 465901 (2017).

[23] P. Giannozzi, O. Baseggio, P. Bonfa, D. Brunato, R. Car, I. Carnimeo, C. Cavazzoni, S. de Gironcoli, P. Delugas, F. F. Ruffino, A. Ferretti, N. Marzari, I. Timrov, A. Urru, and S. Baroni, J. Chem. Phys. **152**, 154105 (2020).

[24] M. Methfessel and A. T. Paxton, Phys. Rev. B **40**, 3616 (1989).

[25] H. L. Zhang, R. Li, Z. N. Cai, Z. Y. Gu, A. A. Heidari, M. J. Wang, H. L. Chen, and M. Y. Chen, Expert Syst. Appl. **159**, 113617 (2020).

[26] B. G. Pfrommer, M. Cote, S. G. Louie, and M. L. Cohen, J. Comput. Phys. **131**, 233 (1997).

[27] A. Floris, I. Timrov, B. Himmetoglu, N. Marzari, S. de Gironcoli, and M. Cococcioni, Phys. Rev. B **101**, 064305 (2020).

[28] J. Heyd, G. E. Scuseria, and M. Ernzerhof, J. Chem. Phys. **118**, 8207 (2003).

[29] G. Kresse and J. Furthmuller, Phys. Rev. B **54**, 11169 (1996).

[30] G. Kresse and J. Furthmuller, Comput. Mater. Sci. **6**, 15 (1996).

[31] See Supplemental Material at http://link.aps.org/supplemental/10.1103/PhysRevB.104.054515 for the electronic band structures and phonon dispersions of LaO using different exchange-correlation functionals, which include Refs. [21–24,27–30,47,60,68–79].

[32] P. B. Allen and R. C. Dynes, Phys. Rev. B **12**, 905 (1975).

[33] A. Sanna, J. A. Flores-Livas, A. Davydov, G. Profeta, K. Dewhurst, S. Sharma, and E. K. U. Gross, J. Phys. Soc. Jpn. **87**, 041012 (2018).

[34] Y. Mizuguchi, H. Takeya, Y. Kawasaki, T. Ozaki, S. Tsuda, T. Yamaguchi, and Y. Takano, Appl. Phys. Lett. **98**, 042511 (2011).

[35] A. D. Becke and K. E. Edgecombe, J. Chem. Phys. **92**, 5397 (1990).

[36] J. R. Rumble, *CRC Handbook of Chemistry and Physics* (CRC Press/Taylor & Francis, Boca Raton, FL, 2021).

[37] S. D. Guo and B. G. Liu, Phys. B **408**, 110 (2013).

[38] F. F. Tafti, M. S. Torikachvili, R. L. Stillwell, B. Baer, E. Stavrou, S. T. Weir, Y. K. Vohra, H. Y. Yang, E. F. McDonnell, S. K. Kushwaha, Q. D. Gibson, R. J. Cava, and J. R. Jeffries, Phys. Rev. B **95**, 014507 (2017).

[39] Y. Shaidu and O. Akin-Ojo, Comput. Mater. Sci. **118**, 11 (2016).

[40] M. F. Thorpe and S. W. de Leeuw, Phys. Rev. B **33**, 8490 (1986).

[41] Z. H. Yang, K. P. Yuan, J. Meng, X. L. Zhang, D. W. Tang, and M. Hu, Nanotechnology **32**, 025709 (2021).

[42] W. Zhong, R. D. King-Smith, and D. Vanderbilt, Phys. Rev. Lett. **72**, 3618 (1994).

[43] J. Sarnthein, A. Pasquarello, and R. Car, Science **275**, 1925 (1997).

[44] A. Raeliarijaona and H. X. Fu, Phys. Rev. B **92**, 094303 (2015).

[45] I. S. Tupitsyn and N. V. Prokof'ev, Phys. Rev. Lett. **118**, 026403 (2017).

[46] B. Rosenstein, H. C. Kao, and M. Lewkowicz, Phys. Rev. B **90**, 045137 (2014).

[47] S. Y. Yue, L. Cheng, B. L. Liao, and M. Hu, Phys. Chem. Chem. Phys. **20**, 27125 (2018).

[48] Y. L. Li, W. Luo, Z. Zeng, H. Q. Lin, H. K. Mao, and R. Ahuja, Proc. Natl. Acad. Sci. (USA) **110**, 9289 (2013).

[49] C. Heil, S. Ponce, H. Lambert, M. Schlipf, E. R. Margine, and F. Giustino, Phys. Rev. Lett. **119**, 087003 (2017).

[50] J. J. Zheng and E. R. Margine, Phys. Rev. B **94**, 064509 (2016).
[51] P. B. Allen and R. C. Dynes, J. Phys. C **8**, L158 (1975).
[52] Y. Y. Li, Y. K. Weng, J. J. Zhang, J. F. Ding, Y. H. Zhu, Q. X. Wang, Y. Yang, Y. C. Cheng, Q. Zhang, P. Li, J. D. Lin, W. Chen, Y. Han, X. X. Zhang, L. Chen, X. Chen, J. S. Chen, S. Dong, X. H. Chen, and T. Wu, NPG Asia Mater. **10**, 522 (2018).
[53] Y. Guo, Y. F. Zhang, X. Y. Bao, T. Z. Han, Z. Tang, L. X. Zhang, W. G. Zhu, E. G. Wang, Q. Niu, Z. Q. Qiu, J. F. Jia, Z. X. Zhao, and Q. K. Xue, Science **306**, 1915 (2004).
[54] M. M. Ozer, Y. Jia, Z. Y. Zhang, J. R. Thompson, and H. H. Weitering, Science **316**, 1594 (2007).
[55] A. I. Gubin, K. S. Il'in, S. A. Vitusevich, M. Siegel, and N. Klein, Phys. Rev. B **72**, 064503 (2005).
[56] C. Liu, C. S. Lian, M. H. Liao, Y. Wang, Y. Zhong, C. Ding, W. Li, C. L. Song, K. He, X. C. Ma, W. H. Duan, D. Zhang, Y. Xu, L. L. Wang, and Q. K. Xue, Phys. Rev. Mater. **2**, 094001 (2018).
[57] L. Kang, B. B. Jin, X. Y. Liu, X. Q. Jia, J. Chen, Z. M. Ji, W. W. Xu, P. H. Wu, S. B. Mi, A. Pimenov, Y. J. Wu, and B. G. Wang, J. Appl. Phys. **109**, 033908 (2011).
[58] R. Yan, G. Khalsa, B. T. Schaefer, A. Jarjour, S. Rouvimov, K. C. Nowack, H. G. Xing, and D. Jena, Appl. Phys. Express **12**, 023008 (2019).
[59] W. H. Tang, C. Y. Ng, C. Y. Yau, and J. Gao, Supercond. Sci. Technol. **13**, 580 (2000).
[60] F. Peng, Y. Sun, C. J. Pickard, R. J. Needs, Q. Wu, and Y. M. Ma, Phys. Rev. Lett. **119**, 107001 (2017).
[61] P. W. Anderson, Science **235**, 1196 (1987).
[62] J. R. Schrieffer, X. G. Wen, and S. C. Zhang, Phys. Rev. B **39**, 11663 (1989).
[63] A. Weidinger, C. Niedermayer, A. Golnik, R. Simon, E. Recknagel, J. I. Budnick, B. Chamberland, and C. Baines, Phys. Rev. Lett. **62**, 102 (1989).
[64] A. J. Millis, H. Monien, and D. Pines, Phys. Rev. B **42**, 167 (1990).
[65] H. Kontani, K. Kanki, and K. Ueda, J. Phys. Chem. Solids **62**, 83 (2001).
[66] S. Uchida, H. Takagi, K. Kitazawa, and S. Tanaka, Jpn. J. Appl. Phys. **26**, L1 (1987).
[67] S. Dzhumanov, Solid State Commun. **115**, 155 (2000).
[68] G. Kresse and D. Joubert, Phys. Rev. B **59**, 1758 (1999).
[69] E. R. Margine, H. Lambert, and F. Giustino, Sci. Rep. **6**, 21414 (2016).
[70] S. Y. Deng, X. Q. Song, X. C. Shao, Q. Li, Y. Xie, C. F. Chen, and Y. M. Ma, Phys. Rev. B **100**, 224108 (2019).
[71] K. Kunc and R. M. Martin, Phys. Rev. Lett. **48**, 406 (1982).
[72] A. Togo, F. Oba, and I. Tanaka, Phys. Rev. B **78**, 134106 (2008).
[73] A. Togo and I. Tanaka, Scr. Mater. **108**, 1 (2015).
[74] A. Patra, B. Patra, L. A. Constantin, and P. Samal, Phys. Rev. B **102**, 045135 (2020).
[75] S. N. Gupta, A. Singh, K. Pal, B. Chakraborty, D. V. S. Muthu, U. V. Waghmare, and A. K. Sood, Phys. Rev. B **96**, 094104 (2017).
[76] Y. B. Zhang, J. W. Sun, J. P. Perdew, and X. F. Wu, Phys. Rev. B **96**, 035143 (2017).
[77] J. Wrobel, K. J. Kurzydlowski, K. Hummer, G. Kresse, and J. Piechota, Phys. Rev. B **80**, 155124 (2009).
[78] K. Hummer, J. Harl, and G. Kresse, Phys. Rev. B **80**, 115205 (2009).
[79] S. A. Seidl, B. Kretz, C. Gehrmann, and D. A. Egger, Phys. Rev. Mater. **5**, 034602 (2021).